Advances in Colloid and Interface Science 292 (2021) 102419

Contents lists available at ScienceDirect

Advances in Colloid and Interface Science

journal homepage: www.elsevier.com/locate/cis

Historical Perspective

Thermoplastic bio-nanocomposites: From measurement of fundamental properties to practical application

Ivanna Colijn *, Karin Schroën

Wageningen University, Food Process Engineering group, Wageningen, the Netherlands

ARTICLE INFO

Available online 16 April 2021

Keywords:
Biodegradable plastics
Nanocomposites
Nanoparticles
Surface energy
Aggregation strength
Interphase region

ABSTRACT

Although the discovery of plastic has revolutionized materials used in many industries and by consumers, their non-biodegradable nature has led to one of the greatest problems of our times: plastic waste in the environment. Bioplastics which are biobased and biodegradable, have been suggested as alternatives for their fossil based counterparts, but their properties often do not meet the requirements that standard plastics would, and are in clear need of improvement.

One way to do so is by the addition of nanoparticles which, when homogeneously dispersed, have been reported to result in great improvements. However, in practice, homogenous distribution of nanoparticles is not that trivial due to their tendency to aggregate, also after addition to the polymer matrix. Although theoretical frameworks to prevent this process are available, we feel that the options explored in practice are often rather trial and error in nature. For that reason, we review the theories available, aiming to facilitate the design of the nanocomposites for a sustainable future.

We first discuss thermodynamic frameworks which revolve around nanoparticle aggregation. To minimize nanoparticle aggregation, the nanoparticle and polymer can be selected in such a way that they have similar polar and dispersive surface energies. The second part is dedicated to nanocomposite processing, where kinetic effects act on the nanocomposite material therewith influencing its final morphology, although it is good to point out that other factors such as reaggregation also affect the final nanocomposite morphology. The third section is dedicated to how nanoparticles affect the polymer matrix to which they are added. We describe how interactions at an atomic scale, result in the formation of an interphasial region which ultimately leads to changed bulk material properties.

From these three sections, we conclude that three parameters are often overlooked when designing nanocomposites, namely the surface energies of the nanoparticles and polymers, the aggregation bond energy or strength, and the interphase region. Therefore, in the fourth section we provide an overview of techniques to identify these three parameters. We finish with a summery and outlook for the design of bio nanocomposites, where we bring all insights from the previous four sections together.

Contents

1. Introduction . . . 2
2. Nanoparticle and polymer selection . . . 2
3. Nanocomposite processing . . . 3
   3.1. Filler addition . . . 3
   3.2. Particle wetting and polymer infiltration . . . 4
   3.3. Aggregate break up and distribution . . . 5
   3.4. Reagglomeration during solidification or annealing . . . 5
   3.5. How to combine thermodynamic and kinetic effects? . . . 6
4. Effect of nanoparticles on polymer . . . 6
   4.1. Nanoparticle-polymer interfacial interactions . . . 6

* Corresponding author at: Wageningen University, Bornse Weilanden 9, 6708 WG Wageningen, the Netherlands.
E-mail addresses: ivanna.colijn@wur.nl (I. Colijn), karin.schroen@wur.nl (K. Schroën).

https://doi.org/10.1016/j.cis.2021.102419

4.2. Formation of an interphase region . . . 6
4.3. Change in bulk properties . . . 8
5. Techniques to investigate nanocomposite systems . . . 8
5.1. Surface energies . . . 8
5.1.1. Direct contact angle measurements . . . 8
5.1.2. Wilhelmy and tilted plate method . . . 9
5.1.3. Inverse gas chromatography . . . 9
5.2. Aggregate strength – Static light scattering . . . 10
5.3. Region of the interphase – atomic force microscopy . . . 10
5.3.1. Peak force tapping mode (PF-TM) . . . 10
5.3.2. Inter modulation AFM (ImAFM) . . . 11
6. Summary and outlook . . . 11
Declaration of Competing Interest . . . 11
Acknowledgements . . . 11
Appendix A. Supplementary data . . . 11
References . . . 11

1. Introduction

For the production of the first plastics, natural materials were used that were eventually modified to reach improved functionality, and in a later stage evolved into completely synthetic polymers that showed remarkable properties in terms of e.g. strength per weight of material used. Currently, synthetic polymers are subject to scrutiny for their environmental impact related to the use of fossil fuels for their production, and low biodegradability. Bio-degradable polymers are therefore gaining more and more interest, although it should also be pointed out that the functionality of these polymers can be rather low compared to their synthetic counterparts. Further functionalization is therefore needed, and in this paper we focus on the use of nano-particles to do so.

The addition of nanoparticles to polymer matrixes has led to extraordinary material properties compared to the base-polymer, such as increased mechanical strength, increased thermal stability, and increased barrier properties [1–7]. In the early days, the focus laid mainly on the automotive and aviation industry, which resulted in the use of nanocomposites in for example tires or conveyor belts. Besides tuning macroscopic polymer properties, it has been suggested that extra functionality, e.g. anti-oxidant or anti-microbial, can be created if the nanoparticle possesses that functionality [8–12]. These latter two aspects are especially of interest for packaging materials for food, or medical applications.

The enhanced properties of nano-composites are related to the high surface area of the nanoparticles, which facilitates interaction with the base polymer. However, not all combinations are successful, in fact, huge differences in final material properties have been reported even when similar starting materials were used. Besides, the properties of the polymer and the particles need to be matched, one of the main challenges is to achieve a homogeneous dispersion of nanoparticles throughout the polymer matrix. This is only possible if particle aggregation, a process driven by fundamental properties of the polymer and the particle, is prevented. Besides that, we feel that clear material – process – structure – property relationships are missing, and that design of a nanocomposite mostly relies on trial and error approaches, also due to the complexity of the processes at hand. In short, designing a nanocomposite with desired properties is far from trivial.

Investigating nanocomposite systems is a challenge in itself due to the small size of the nanoparticles which asks for advanced techniques. Still, a lot of knowledge is available, which we try to compile that in this review. The first section is dedicated to particle and polymer properties, and revolves around thermodynamic arguments. In the second section, we highlight process-related aspects that revolve around kinetic effects that play a role, e.g. in aggregation. In the third section we focus on how nanoparticle – polymer interactions affect material properties on different length scales. The fourth section is dedicated to techniques to quantify several design parameters as identified in the earlier three sections. We will wrap up with a section in which we bring the insights presented in the previous sections together as an outlook for the design of bio-nanocomposites.

2. Nanoparticle and polymer selection

Nanoparticle and polymer selection is a crucial step in nanocomposite design because nanoparticles can significantly change material properties. To maximize their effect on the polymer matrix, one should achieve a homogeneous dispersion, which is generally considered the main challenge in nanocomposite development and design.

For homogeneous dispersion given equilibrium conditions, the interfacial compatibility between the filler and the polymer plays a crucial role. From a thermodynamic point of view, the free energy can be used to determine whether a process may take place. For nanocomposites, the free energy of immersion (ΔG_i), can be used to quantify whether the dispersed state is favored over the non-dispersed state [13] (Fig. 1).

$$\Delta G_i = \gamma_{pf} - \gamma_{ff} \quad (1)$$

Here, γ_{pf} is the interfacial energy in J/m^2 between the polymer and the filler and γ_{ff} is the surface energy of the filler alone J/m^2. When

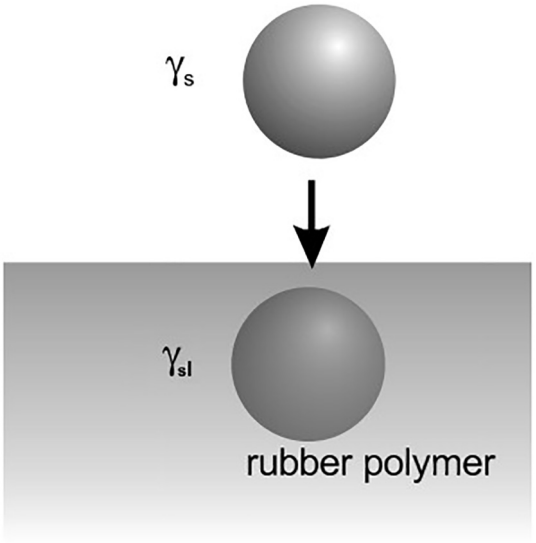

Fig. 1. Schematic representation of the free energy of immersion. Retrieved from [13].

ΔG_i is <0, the dispersed state is favored and when $\Delta G_i > 0$ the non-dispersed phase is favored.

The γ_{pf}-part of the equation can be calculated using the surface energies of the filler and polymer (which is also related to the contact angle, see section "4.1 Surface energies"). The total surface energy of a compound is the product of a dispersive component (γ^d) and a polar component (γ^p). The dispersive component represents interactions due to London's dispersive forces whereas the polar component represents the polar functional groups such as the hydroxyl or amino moieties. The total surface energy can be described as:

$$\gamma = \gamma^d + \gamma^p \tag{2}$$

Implementing Eq. (2) in Eq. (1) gives the following relationship between the free energy of immersion as function of the dispersive and polar components of the filler and the polymer, respectively [13]:

$$\Delta G_i = \gamma_p - 2\left(\sqrt{\gamma_f^d \gamma_p^d} + \sqrt{\gamma_f^p \gamma_p^p}\right) \tag{3}$$

where γ_f^d and γ_p^d are the dispersive components of filler and polymer, respectively, and γ_f^p and γ_p^p the polar components. Eq. (3) indicates that the polar and dispersive components of the filler and the polymer should be similar in order to allow spontaneous dispersion of the filler in the polymer matrix.

Stöckelhuber et al. [13] used this approach for rubbers in combination with different fillers including silica and nanoclays. Most ΔGi's were strongly negative, and could be correlated to the free energy of immersion and different dispersibility behaviors, although there are some doubts about the actual values that were obtained. Tang et al. [14] modified attapulgite to improve its compatibility with EPDM (ethylene-propylene-diene monomer). Although a decline in the free energy of immersion did not directly lead to a decreased aggregate size, it could be correlated to an increased tensile strength, i.e. improved mechanical properties.

Alternatively, the work of adhesion between filler-filler and filler-polymer has been suggested by Natarajan, Li et al. [15] who showed that the ratio between the work of adhesion of the filler-polymer (W_{FP}) needs to be higher than the work of adhesion between the filler particles (W_{FF}). Similarly as the free energy of immersion, W_{FP}/W_{FF} can be calculated using the dispersive and polar components Eq. (4).

$$\frac{W_{PF}}{W_{FF}} = \frac{2\left(\sqrt{\gamma_f^d \gamma_p^d} + \sqrt{\gamma_f^p \gamma_p^p}\right)}{2\gamma_f} \tag{4}$$

Natarajan, Li et al. [15] found consistent relationships between W_{PF}/W_{FF} and the dispersion of different silica nanoparticles in polystyrene, poly(methyl methacrylate), poly (ethyl methacrylate), and poly(2-vinylpyridine). Khoshkava & Kamal [16] used the same approach to investigate modified cellulose nanocrystals in poly lactic acid and poly propylene. Also here an increased W_{PF}/W_{FF} was indicative of improved dispersibility, although this could not be related to aggregate size. Interestingly, these results correspond well to molecular dynamic simulations which show that the interaction strength of filler–polymer and filler–filler were the dominant enthalpic factors for dispersion of nanoparticles in a polymer melt [17].

Whether one uses ΔG_i, W_{PF}/W_{FF}, or another comparable approach, generally having a similar polar and dispersive component in nanoparticle and matrix is a good approach to improve nanoparticles dispersion [18–20]. Obviously, this limits the combinations that can be considered greatly, therefore modification of either the particle or the polymer is a viable way to extend the options for nanocomposite production. For example, L. Zhang et al. [18] modified carbon black nanoparticles and found improved dispersion when the surface energies were similar as poly lactic acid, and Gan et al. [20] tuned surface acetylation of cellulose nanocrystals to match poly (3-hydroxybutyrate-*co*-4-hydroxybutyrate). These are only a couple of examples; many papers discuss possible modification routes, for instance [21–24].

3. Nanocomposite processing

In the previous section we have presented a theoretical framework for (modified) nanoparticle selection based on thermodynamic arguments. However, in practice this may not be the determining factor to achieve a homogeneous dispersion of nanoparticles in the polymer matrix. Nanoparticles may get physically trapped in a solidified polymer, thus leading to a kinetically arrested system that has not reached thermodynamic equilibrium [25]. Which of the aspects contributes most to the actual product also depends on the production method, and those are elaborated in this section.

In general, three different production methods can be distinguished, i.e. solvent casting, melt mixing, and in situ polymerization. During solvent casting, the nanoparticles and polymer are added to a solvent after which the mixture is 'poured' into a mould. As it takes some time until all solvent is evaporated, both thermodynamic and kinetic arguments are expected to be relevant, depending on the removal rate of the solvent. During in situ polymerization, the nanoparticles are either added to a solution with the monomer or to the monomer itself. The polymerization process starts at the surface of the particles triggered by a catalyst, which can be an external initiator, heat, or radiation [26,27]. In contrast to the solvent casting and melt mixing process, a covalent bond is formed. This has shown to improve the dispersibility in the polymer matrix [28,29], as potential nanoparticle aggregates were torn appart during the reaction [30]. For the product made, both the (modified) thermodynamic, and kinetic considerations are of importance. During melt mixing, nanoparticles are added to a polymer melt under high shear forces. Often a twin screw extruder is used to promote dispersion of fillers [31]. Compared to in situ polymerization and solvent casting, kinetics is expected to play the biggest role in melt mixing as the material is directly solidified after production. In industry, melt mixing is by far the most used processing method because it is relatively environmentally friendly, cost effective, and industrially viable [27]. For that reason, we mainly consider melt-mixing based on extrusion in the next section.

The relevant processes in an extruder can be sub-divided into different phases as presented in Fig. 2, during which:

1. Nanoparticles are added to the polymer melt.
2. The nanoparticle surface is wetted by the matrix and depending on the interfacial compatibility, the polymer may infiltrate the aggregates. The latter process is sometimes referred to as intercalation.
3. Nanoparticle aggregates break up and are 'homogeneously' dispersed in the matrix.
4. Depending on the interfacial compatibility and the solidification time, reaggregation may occur.

3.1. Filler addition

In general, there is a continuous competition between thermodynamics driving the particles together and kinetics breaking the aggregates up, which leads to a certain aggregate size [32]. Móczó & Pukánszky [33] described this mathematically:

$$\frac{F_a}{F_h} = k\,\frac{W_{AB}}{\eta \dot{\gamma} R} \tag{5}$$

where F_a/F_h is the ratio between the adhesive forces and hydrodynamic forces acting on a nanoparticle aggregate, W_{AB} is the reversible work of adhesion between particles in an aggregate, $\dot{\gamma}$ is the shear rate, η is the melt viscosity, and R is the aggregate radius or in ideal cases the radius of the individual nanoparticles.is the particle/aggregate size.

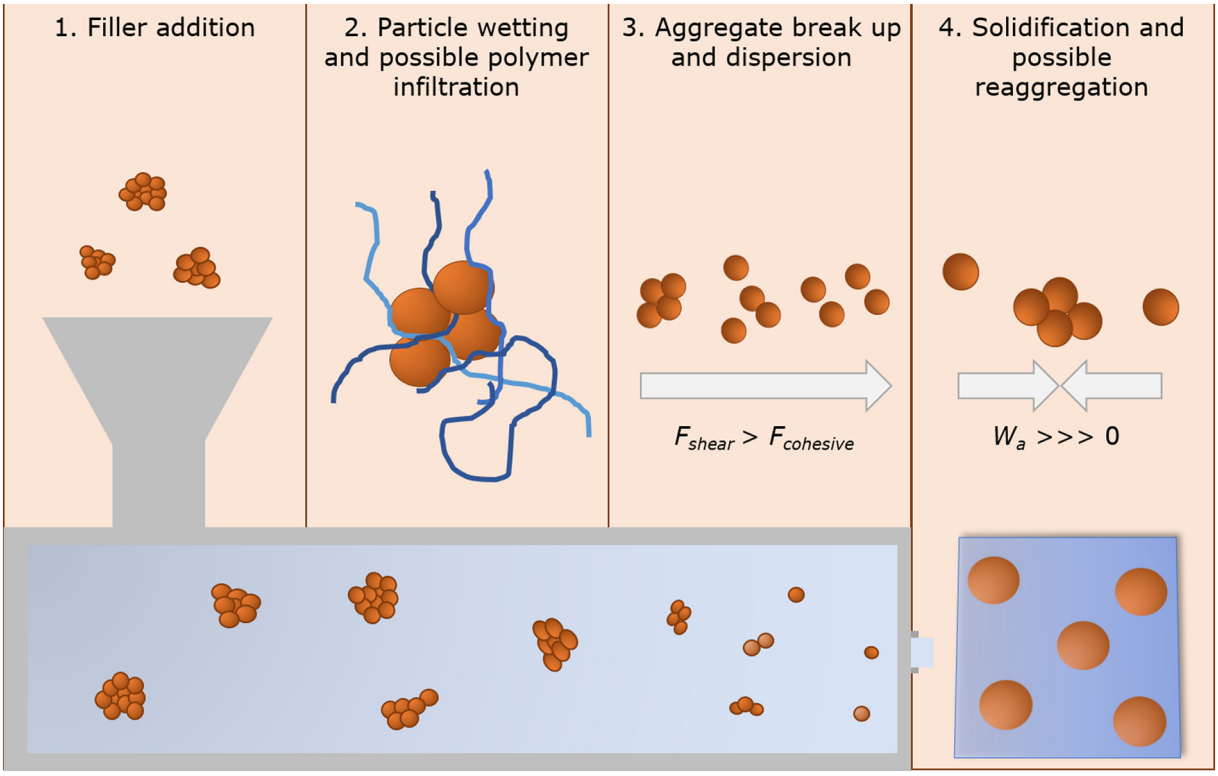

Fig. 2. Different processes occurring in an extruder where 1) nanoparticle addition 2) particle wetting and the surrounded polymer infiltrating the nanoparticle aggregates 3) nanoparticle aggregate beak up provided that the applied shear forces are higher than the cohesive shear forces 4) solidification and possible reaggregation when the work of adhesion is much larger than 0.

Separating R gives:

$$R = k^* \frac{W_{AB}}{\eta\gamma} \frac{F_h}{F_a} \tag{6}$$

Eq. (6) basically suggests that the final morphology of a nanocomposite depends on the kinetic and adhesive forces acting, rather than the initial state of the nanoparticles, e.g. a powder or dispersion. Experimentally this has been confirmed by Gaspar et al. [34] who investigated the morphology of different fullerene C60 formulations along the axis of a twin screw extruder. The final morphology was mainly driven by thermodynamics and flow conditions, and particle pre-treatment was less important.

However, in practice the equilibrium size is seldomly reached, considering the commonly applied shear rates and short residence times in an extruder. To improve dispersion, it is expected that interfacial compatibility is the most important design parameter, that is, in combination with certain process conditions. Nevertheless, the actual preparation of the nanoparticle may play a role as pointed out by for instance, Khoshkava & Kamal [35], who found a smaller aggregate size in poly propylene nanocomposites when the cellulose nanocrystals were spray dried instead of freeze dried, which is expected to have influenced the porosity of the particles [35–37]. Obviously, starting from a smaller initial aggregate size is beneficial, as this is closer to the final desired morphology Furthermore, it was found that dispersibility improved by increasing the porosity of the nanoparticle aggregates [37,38] as also discussed in the next section.

3.2. Particle wetting and polymer infiltration

The nanoparticle surface can be wetted by the polymer melt provided that the interfacial compatibility is beneficial. Whether this is the case is determined by the contact angle (θ), which is 0° in case of complete wetting, but has a finite value in most practical systems. The contact angle can be calculated from the surface energies of the filler and polymer [39,40]:

$$\cos\theta = -1 + 2\frac{\sqrt{\gamma_P^d \gamma_F^d}}{\gamma_F} + 2\frac{\sqrt{\gamma_P^p \gamma_F^p}}{\gamma_F} = -1 + 2\frac{W_{PF}}{W_{FF}}$$

$$\cos\theta = \begin{cases} -1 + 2\dfrac{W_{PF}}{W_{FF}} & \dfrac{W_{PF}}{W_{FF}} < 1 \\ 1 & \dfrac{W_{PF}}{W_{FF}} \geq 1 \end{cases} \tag{9}$$

Please note that the interfacial properties discussed in the thermodynamics section co-determine the contact angle. A contact angle ~0° implies better particle dispersibility.

Whether polymer infiltration due to capillary effects plays an important role, depends on nanoparticle and polymer properties. Generally, capillary rise can be described by the Lucas-Washburn equation:

$$H(t) = \sqrt{\frac{\gamma_{polymer}\, r\, t\, \cos\theta}{2\eta}} \tag{10}$$

where H is the rise of a fluid (in our case a molten polymer), r is the pore radius of the nanoparticle aggregate, θ is the contact angle between the meniscus and the wall, η is the viscosity of the fluid (in our case a molten polymer), and t is the wetting time.

Depending on the properties of the nanoparticle and polymer, capillary forces may be very significant, or not at all important. To illustrate this, we consider magnesium carbonate nanoparticles with an aggregate size of 30 nm leading to pore sizes between 1 and 10 nm [41]. When completely wetted ($\theta = 0°$) and added to a polymer melt with viscosity of 600 Pa·s, the capillary rise H = 3 μm after 60 s, which

implies that the polymer can penetrate the whole nanoaggregate. This also illustrates the size of aggregates that are expected to be affected by polymer intrusion, and which ones are not or hardly. We are aware that capillary forces are sometimes mentioned, but in most cases they play a minor role because of the high viscosity of the polymer melt in combination with small pore sizes and the short times available for intrusion to take place. Still, in some applications for instance carbon nanotubes capillary forces are relevant, and are sometimes even used in the production of nanocomposites [42].

To be complete, we would like to mention that the suitability of the Lucas-Washburn equation for effects occurring at nanoscale has been questioned by some [43,44], although molecular dynamics studies [42,45], and experimental studies [46] have found good agreement between the Lucas-Washburn equation and capillary forces on nanoscale.

3.3. Aggregate break up and distribution

Since nanoparticle aggregates are often the starting point for nanocomposite production, both dispersion and distribution of nanoparticles through the polymer melt are of importance. The molten polymer is transported through the extruder at high shear [31], which in turn leads to nanocomposite dispersion.

Obviously, the higher the shear forces the higher the probability an aggregate will break up. The dimensionless number Prob has been used to described this [47–49]. A general expression for this probability can be written as:

$$\text{Prob} = e^{\frac{-\sigma}{\tau}} \tag{11}$$

where σ is the cohesive strength of the aggregate and τ is the shear stress of the medium. The cohesive strength of the aggregate is dependent on for example the size of the particles as well as the cohesive forces including van der Waals or hydrophobic forces [47]. Unfortunately, $\sigma_{aggregate}$ is not often quantified, yet could provide much insight because the extrusion process can be tailored in such a way that the shear forces are higher than that. The shear stress is the product of the polymer viscosity η_P and the medium strain rate γ.

$$\tau = \eta_p\, \gamma \tag{12}$$

The medium strain rate depends on the geometry of the extruder. For a concentric cylinder the relationship between geometry and medium strain rate is as follows:

$$\gamma = R\omega/h \tag{13}$$

where R is the radius of the housing, w is the rotational speed of the mixing blade (rad/s) and h is the spacing between the inner wall of the housing and the edge of the mixer blade.

Relationships as shown in Eq. (13), can also be described in terms of energy input (E_{input}) required to overcome the bond energies within an aggregate ($E_{aggregate}$):

$$Prob = e^{\frac{-E_{aggregate}}{E_{input}}} \tag{14}$$

For extrusion processing, E_{input} is commonly described in terms of the specific mechanical energy (SME) that is used to compare the impact of different processing conditions on the nanocomposite material. The SME (in kWh) can be calculated using:

$$SME = \frac{P_{motor}}{\tau_{max} N_{max}} * \frac{\tau\, N}{Q} \tag{15}$$

where τ is the drive motor torque, N is the screw rotation speed, and Q is the flow rate. Although $F_{cohesive}$ or $E_{aggregate}$ are rarely determined, qualitatively it is well known that a certain energy barrier needs to be overcome before dispersion occurs, and many large scale experiments have found a decreasing aggregate size upon increasing SME [50–54]. However, finding experimental proof can be rather unpractical, especially for newly developed materials for which the amount of nanoparticles may be limited in relation to what would be needed for a typical extrusion experiment, and of which the production process would also not be optimized.

To get an impression of whether full dispersion is possible it is recommended to determine $E_{aggregate}$ or $F_{cohesive}$ using a small scale. Recently, we have developed such a method, which is further discussed in section "Aggregate strength – Static light scattering" [55] We found an $E_{aggregate}$ of ~370 kJ / g chitin nanocrystal aggregates. Van der Waals interactions and hydrogen bonds are believed to be the most important interactions within a chitin nanocrystal aggregate. In addition we could also quantify a critical energy barrier of ~100 kJ/g chitin nanocrystals, which can be determined as the minimal energy needed before disintegration occurs. Commonly about 0.17–0.27 kWh/kg is applied during extrusion. Considering a filler content of 5 wt% and a maximum residence time of 10 min, a maximum E_{input} of ~1 kJ/g material can be achieved. This means that about ~50 J/g chitin nanocrystals is available for aggregate break down, assuming that the energy is distributed equally. This value is a factor 2000 lower than the critical energy barrier we identified before. We believe that this is one of the reasons why it remains difficult to achieve a homogeneous dispersion of chitin nanocrystals through polymer matrix without surface modification. Still, one should be cautious in translating these results to larger scale given that the processes taking place in an extruder are very complex. For example, it is well known that the screw configuration can tailor the amount of mechanical mixing, the residence time, and pressure levels, and these are only partly considered in the SME approach [56,57].

3.4. Reagglomeration during solidification or annealing

Besides all previously mentioned arguments, it is good to point out that there is a continuous thermodynamic force driving the nanoparticles to re-agglomerate both in (aqueous) dispersions and in polymer melts [32,37,58,59]. This is nicely demonstrated by Vilaverde et al. [59] who investigated the dispersion and re-agglomeration of graphite nanoplatelets in polypropylene melts. During the extrusion process, the feed stream passes through different extrusion chambers. Early on in the extrusion process (denoted as channel 0–5 in (Fig. 3)), a decreasing particle size was observed (Fig. 3). However, once the material entered the relaxation chamber where no kinetic force was applied, the particle size rapidly increased to its original size, emphasizing that continuous force needs to be applied to maintain homogenous dispersion in a polymer melt. Interestingly, in the same work, the particle size decreased faster in chambers 6–10, compared to the initial dispersion phase, which is indicative of easier re-dispersion.

After extrusion, the nanocomposite material is solidified, which may also include time to anneal if the time for reaggregation is smaller than for solidification. According to Wang and Keddie [60], the tendency of two particles to reaggregate can be described by the difference in work of adhesion (ΔW_a). Similarly as the Gibbs free energy (ΔG_i) of Eq. (3) or W_{FP}/W_{FF} of Eq. (4), these calculations are based on the dispersive and polar components of the filler and polymer:

$$\Delta W_a = 2*\left(\sqrt{\gamma_F^d - \gamma_P^d}\right)^2 + 2*\left(\sqrt{\gamma_F^p - \gamma_P^p}\right)^2 \tag{16}$$

A $\Delta W_a \approx 0$ has been associated with homogenous dispersion, and a high ΔW_a with a large driving force of reagglomeration [13]. In practice, ΔW_a is always positive, because it is very unlikely that the polar and dispersive component of the nanoparticle and polymer completely match. This implies that all nanoparticles will eventually form agglomerates given sufficiently long time. It is good to point out that ΔW_a is no indicator for the aggregate size, as that is also determined by the mobility of the aggregates as a consequence of their size and medium viscosity.

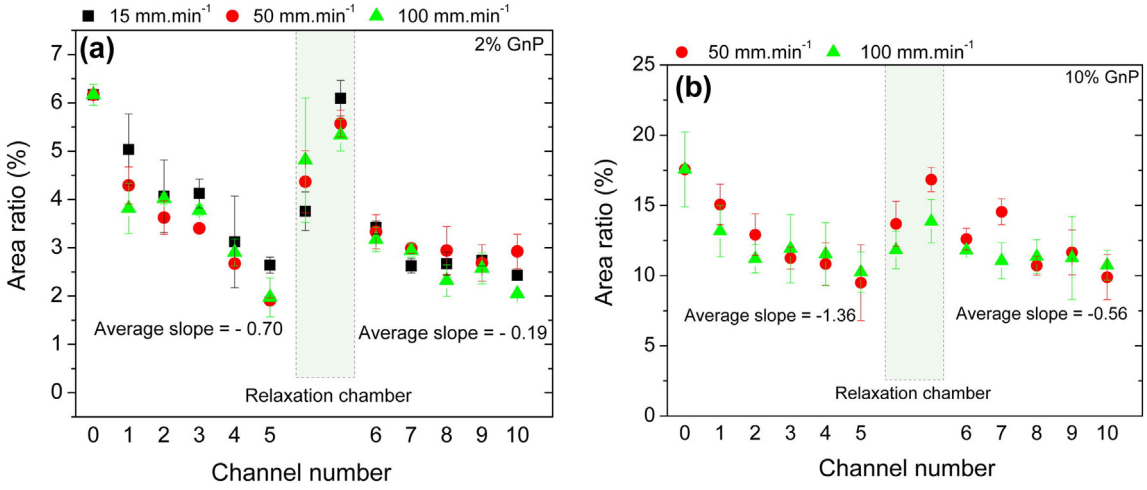

Fig. 3. The evolution of particle size (area ratio (%)) for nanocomposites containing 2 wt% graphene nanoplates prepared at different speeds. The area ratio of the fillers was determined with image analysis of transmission electron microscopy pictures. Retrieved from [59].

3.5. How to combine thermodynamic and kinetic effects?

To summarize, the final structure of a nanocomposite is the result of thermodynamic and kinetic events, and thus both should be considered when designing a nanocomposite material. Hassinger et al. [52] made a first step toward a quantitative tool for predicting dispersion of nanocomposites under non-equilibrium conditions. They tried to describe the final dispersion state of the nanoparticles by the interfacial compatibility between the nanoparticles and polymer (W_{PF}/W_{FF}) and the applied mixing energy in J/s. As hypothesized, their results indicate that the dispersion quality was dependent on both parameters, though a stronger dependency of compatibility between polymer and particle was found. Using data mining techniques, these authors tried to develop a mathematical expression which could predict the final morphology of a nanocomposite based in its compatibility and the applied energy. However, they found that another parameter needed to be included as well, i.e. *f(matrix)*, which describes the mobility and crystallinity of the polymer matrix. The first step toward a predictive tool is very valuable but also emphasizes the complexity of the development of nanocomposite materials.

4. Effect of nanoparticles on polymer

In the previous two sections we have presented different ways to look at dispersibility of nanoparticles in the polymer matrix, i.e. using thermodynamic and a kinetic arguments. In this section we will focus on nanoparticle – polymer interactions and how this affects the material properties at micro and bulk scale (Fig. 4).

4.1. Nanoparticle-polymer interfacial interactions

Nanoparticles and polymers can interact in different ways with covalent interactions, hydrogen bonding, and van der Waals interactions considered to be of most important for nanocomposites. To determine the dominating interaction in a certain nanocomposite, the functional groups of the nanoparticles and the matrix of choice need to be considered.

Covalent interactions (formed during in-situ polymerization or cross linking) have proven to effectively improve nanocomposite properties e.g. mechanical strength [28,29]. Two main reasons could be ascribed to this. First, covalent bonds are very strong (up to 200 k_BT) especially compared to hydrogen bonds or van der Waals interactions that amount to ~10 and ~ 1 k_BT, respectively [61]. Second, an improved nanoparticle dispersibility has been observed because potential aggregates could be torn apart during the reaction [28–30]. Thus for these systems it is likely that covalent bonds are the most dominant interfacial interactions, and drive product improvement, though hydrogen bonds and van der Waals interactions could contribute as well. For example, Shen et al. [62] added silver graphene oxide nanoparticles to a polylactic acid matrix. Nanocomposites prepared via in-situ polymerization showed better mechanical and antibacterial properties compared to melt blending, while both techniques resulted in better properties compared to the neat poly lactic acid. Luong et al. [63] added graphene sheets to polyimide matrix via in situ polymerization. The Young's modulus increased by approximately 30% at only 0.38 wt% filler addition.

Though hydrogen bonds and van der Waals interactions are weaker compared to covalent bonds, significant improvements can also be found in nanocomposites if these interactions dominate. The addition of 1 wt% chitin nanocrystals increased the tensile strength of maize starch films from 1.64 MPa to 3.69 MPa [64]. Also in polyurethane silica nanocomposites, the enhanced thermal and mechanical properties were related to hydrogen bond formation between silanol groups on nanoparticles and the ester and carbonyl groups in the soft segments [65–68]. Obviously, if hydrogen bonds are dominant, both the nanoparticles and the polymers should have functional groups which can either accept or donate protons. The number and nature of the hydrogen bonds seems to be of importance for the reinforcement [69]. Even nanocomposites of which the reinforcement is entirely dependent on van der Waals interactions have been described in literature. A great example are unfunctionalized carbon nanotubes added via melt blending. Experimental [70] and modeling studies [71,72] showed these systems solely rely on van der Waals interactions [73–75].

Please note that in contrast to most colloidal systems, ionic interactions are not considered for most nanocomposites systems. The conductivity of most plastic polymers is extremely low, and for that reason it is not likely that ionic interactions play a significant role if any. However, ionic interactions could play an important role during the production of nanocomposites, especially if water is present [76,77].

4.2. Formation of an interphase region

It is widely accepted that the mobility of the interfacial polymer changes as a consequence of the previously discussed interfacial interactions, which ultimately changes bulk properties. For this, the strength of the interfacial forces is also of importance, as it influences to which extent the interfacial polymer is restricted [15,33,78–80].

The region at which one single nanoparticle has an influence on the polymer matrix is called the interphase (Fig. 4), and here the properties

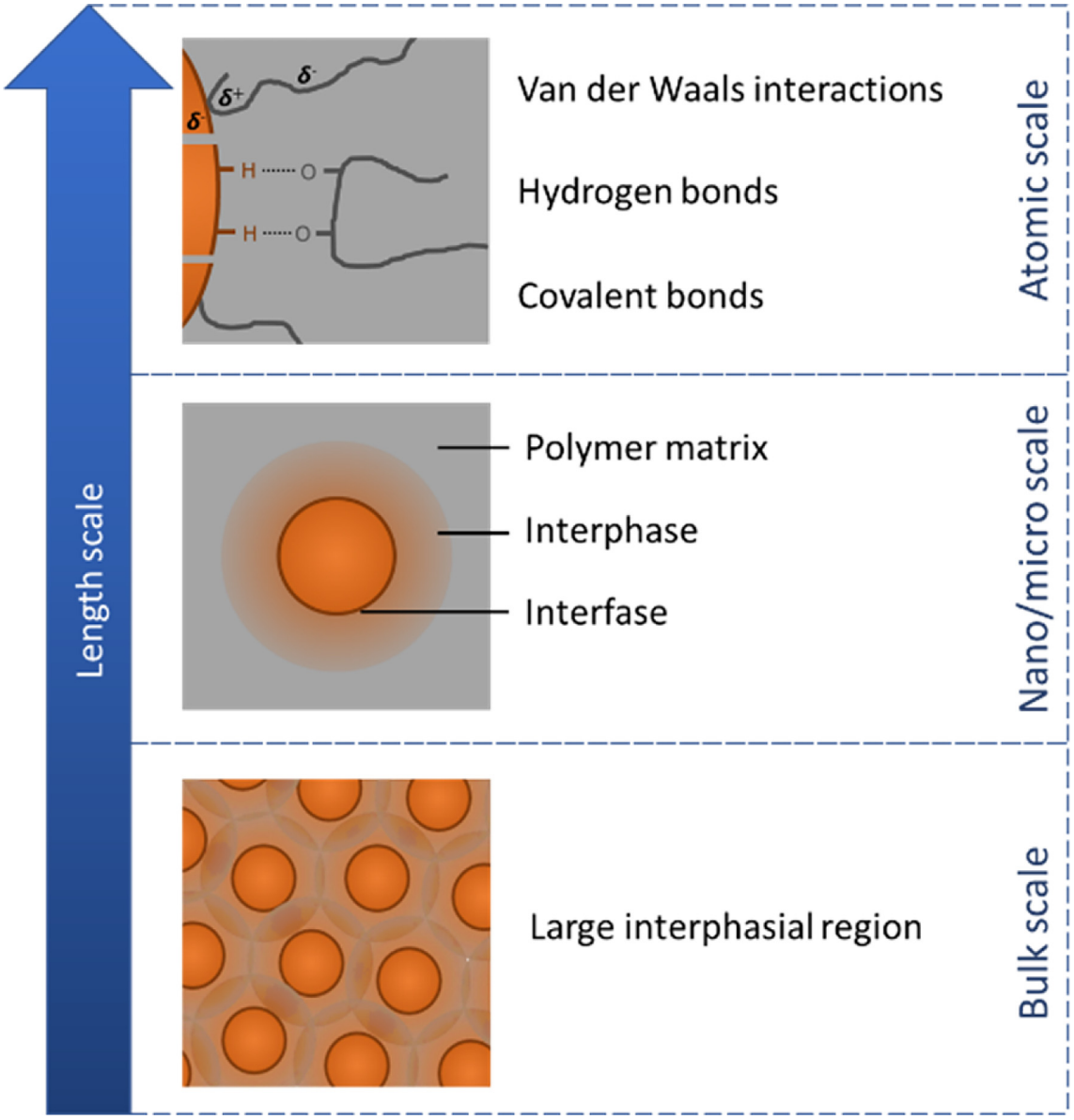

Fig. 4. Schematic overview of nanoparticle interactions at different length scales. Van der Waals interactions, hydrogen bonds, and covalent interactions occur at an atomic level, which results in the formation of an interphase with different properties compared to the nanoparticles and polymers alone. When homogeneously dispersed, this leads to a larger interphasial region, with changed bulk properties.

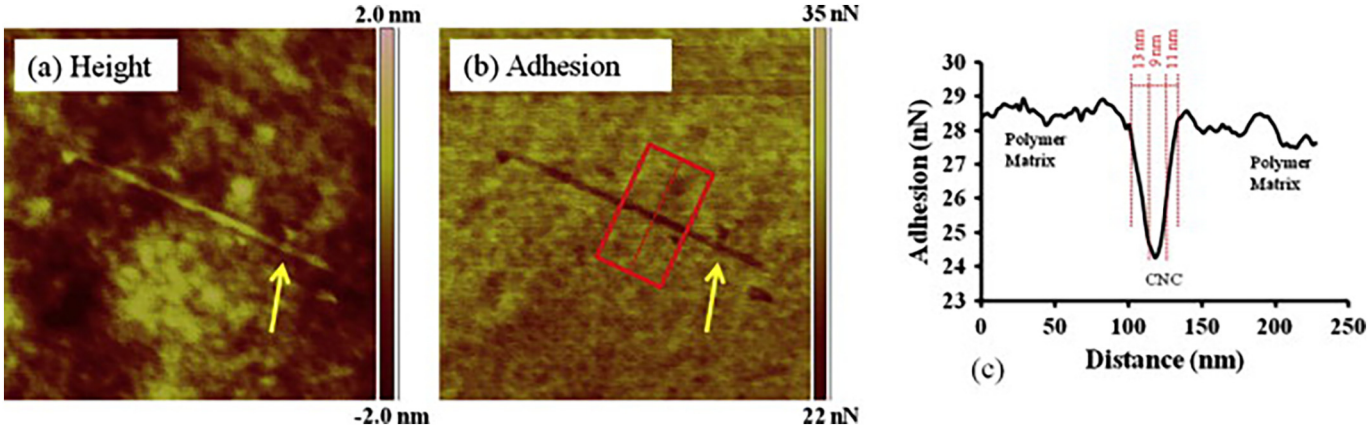

Fig. 5. a) Height and b) adhesion maps showing a single cellulose nanocrystal (marked with yellow arrows) c) Average adhesion profile of the area shown by red rectangle in the adhesion map in b. Using this profile, CNC diameter (9 nm) and average interphase thickness were measured. Retrieved from [69].

of the material are different than that of the polymer or the nanoparticles. To date, atomic force microscopy (AFM) is the only way to directly visualize and quantify the length of the interphase region. One example is the study of Pakzad et al. [69] where they investigated the effect of cellulose nanocrystals crosslinked to a polyvinyl alcohol matrix via polyacrylic acid (Fig. 5). By using the peak force tapping mode, the adhesion force between the AFM tip and the nanocomposite was related to the polymer, the nanoparticles, and the interphasial region. It was found that the thickness of the interphase varied between 4 and 35 nm, depending on the particle diameter. This was explained by an increased surface area which can give rise to a thicker interphase [69,81,82]. This effect was also observed with molecular dynamic simulations, however Phys et al. [83] found that the thickness of the interfacial region is only sensitive to the nanoparticle size when the interfacial interactions are strong.

Also others used atomic force microscopy to quantify the interphase: Houssat et al. [84] for polyimide silicon nitride nanocomposite with particles with a size of 20–40 nm which resulted in an interphase thickness of 27.25 nm, and Hui Huang et al. [85] found that the interphase of 40 nm sized silica particles could reach 55–70 nm in a poly(ethyl methacrylate) and poly(isobutyl methacrylate) matrix. Depending on the particle and polymer properties, the size of the interphase can vary from nanometres to around a micrometre in a heterogeneous gradient system [69,86–88].

4.3. Change in bulk properties

Though the region of the interphase is relatively small (several nanometres up to ~1 μm), it is important to realize that the effects that occur in this region are responsible for improvements at bulk scale. Considering the small size of nanoparticles, and high specific surface area, a significant volume of nanoparticle – polymer interphase is created. This implies that even at low particle loadings much of the bulk material could be considered an interphasial region, leading to bulk properties being dominated by the material properties in this region. In fact, there are even indications that the enhancement of stiffness increases by 5% at the midpoint of two interphasial regions, suggesting these effects may be additive [89].

Keeping this in mind, it is logical that bulk properties change, and this has been extensively reported for many different types of particles [1–7]. Commonly reported enhancements include increased mechanical strength and improved barrier properties [1–7,90]. To stress the importance of the interphasial region, it is important to mention that in different numerical, mathematical, simulation models the interphasial region is used to predict product properties, for instance in the intensity model of Lewis [91], or the multi-core model of Tanaka [92], although many more exist [93–99].

To prevent any confusion, it is good to point out that the degree of crystallinity (X%) is an indicator for polymer mobility at bulk scale. However, increased interphasial region stiffness, does not necessarily lead to increased crystallinity; this could be the result of a nucleating effect as reported for amongst others cellulose nanocrystals [100], carbon nanotubes, and nanoclays [101–103]. When homogeneously dispersed, nanoparticles provide nucleation sites which accelerate polymer crystallization.

Natarajan et al. [15] proposed an experimental approach to predict whether a nanoparticle – polymer combination results in improved properties. They based their method on the hypothesis that for a polymer to spread spontaneously on the filler surface, the relative attraction of the monomeric units needs to be higher than the cohesive attraction in the bulk [104]. This could be described by the ratio between the work of adhesion between the filler-polymer and the polymer-polymer, i.e. the work of spreading W_s:

$$W_s = 2\left(\sqrt{\gamma_P^d \gamma_F^d} + \sqrt{\gamma_P^p \gamma_F^p}\right) - 2\left(\gamma_P^d + \gamma_P^p\right) \tag{17}$$

A W_s of ≥0 suggests an attractive interaction between polymer and filler and should therefore result in a decrease in polymer mobility. When W_s is ≤0, the polymer – polymer interaction is stronger, and no effect on polymer mobility should be visible. Using this approach, good correlations between increased W_s and an increased glass transition temperature were found [15].

5. Techniques to investigate nanocomposite systems

As is clear from the previous sections, designing a nanocomposite with desired properties is far from trivial. Nevertheless, the presented theoretical frameworks supply a lot of insight on compatible particle / polymer combinations that allow creation of a homogeneous nanoparticle distribution, resulting in the formation of an interphase region and ultimately in improved bulk properties. The nanoparticle and polymer surface energy, $F_{cohesive}$ and $E_{aggregate}$, and the thickness of the interphase are key for that, and in this section we discuss different techniques to quantify these parameters.

5.1. Surface energies

The surface energy has shown to be a crucial parameter for the quantification of the interfacial compatibility between nanoparticle and polymer matrix. Amongst others, free energy of immersion (Eq. (3)), the ratio between the work of adhesion of the filler-polymer and the work of adhesion between the filler particles (Eq. (4)), and the work of adhesion (Eq. (18)) were previously mentioned. In these equations a division of the total surface energy into a dispersive and a polar component (Eq. (2)) is used, which can be quantified with different methods such as direct contact angle measurement, the Wilhelmy method, or inverse gas chromatography. In Table SI 1, we give an overview of the various values that we found in the consulted references, and that we compiled to give our readers direct access to values that can be used in nano-composite design. It is clear that the actual values vary greatly, as is the split between polar and dispersive components. Further, the surface energy is temperature dependent [105]; e.g., organoclay had higher surface energies than HDMP and PS at room temperature, but the situation was reversed at processing temperature [106].

5.1.1. Direct contact angle measurements

Contact angle measurement is one of the most common techniques to determine the surface properties of solids. It uses the contact angle between a surface (e.g. a plastic film or a pellet of nanoparticles) and the edge of a liquid droplet, which amongst others gives information about the hydrophobicity and wettability of a certain surface.

For solids the surface energy can only be derived indirectly, and different methods can be used, for instance Fowkes [107] and Owens-Wendt [39]. We take the Owens-Wendt approach as an example, which considers the surface free energy as the sum of a dispersive and polar component (Eq. (2)). The surface energy and individual components for a material of choice can be calculated using at least two liquids of which these previously mentioned dispersive and polar values are known. The dispersive (γ_s^d) and polar component (γ_s^p) of the material of choice can be calculated using:

$$\left(\gamma_s^d\right)^{0.5} = \gamma_i(\cos\theta_i + 1) - \sqrt{\frac{\left(\gamma_i^p/\gamma_j^p\right)\gamma_j(\cos\theta_j + 1)}{2\left(\sqrt{\gamma_i^d} - \sqrt{\gamma_i^p}\left(\frac{j}{\gamma_j^d}\right)\right)}} \tag{18}$$

And

$$(\gamma_s^p)^{0.5} = \frac{\gamma_j(\cos\theta_j + 1) - 2\sqrt{\gamma_s^d/\gamma_j^d}}{2\sqrt{\gamma_j^p}} \quad (19)$$

where γ_i and γ_j are the total surface energies of liquid i and j, γ_i^p and γ_j^p are the polar component of liquid i and j, γ_i^d and γ_j^d are the dispersive component of liquid i and j, and θ_i and θ_j are the contact angles of liquid i and j respectively.

Although the contact angle technique is a relatively straight forward approach, it's accuracy relies on many factors including the surface rigidity, surface roughness, physical and chemical homogeneity, and surface impurities. The influence of each of these factors are discussed in [108,109].

5.1.2. Wilhelmy and tilted plate method

Like direct contact angle measurements, also the Wilhelmy method and the tilted plate method use a contact angle to determine the surface free energy. In case of the Wilhelmy method, particles are fixed at a double-face adhesive plate and immersed and withdrawn from different solutions. The advancing contact angle during immersion of the plate (θ_a), and the receding contact angle (θ_r) during withdrawal are measured (Fig. 6A). In case of the tilted plate method, the nanoparticles are fixed on a plate on which a sessile droplet is formed. When the plate is tilted, an advancing contact angle is formed at the bottom of the drop, and a receding contact angle is formed at the upper side of the drop (Fig. 6B). Just like the direct contact measurements, the individual components of the total surface energy can be calculated with the Owens-Wendt Eqs. (18), (19).

5.1.3. Inverse gas chromatography

Inverse gas chromatography (IGC), has shown to be a valuable tool for the characterization of surface and bulk properties of solid materials including nanoparticles and polymer plastics. One of its most used applications, is for the quantification of the surface free energy [110].

Two methods exist to determine the dispersive and polar component of a sample, i.e. the Dorris-Gray [111] and Schultz method [112]. Here, we only present the Dorris-Gray method because it has shown to be the more accurate [113]. For information on the Schultz method or IGC in general we refer to the review of Mohammadi-Jam and Waters [110].

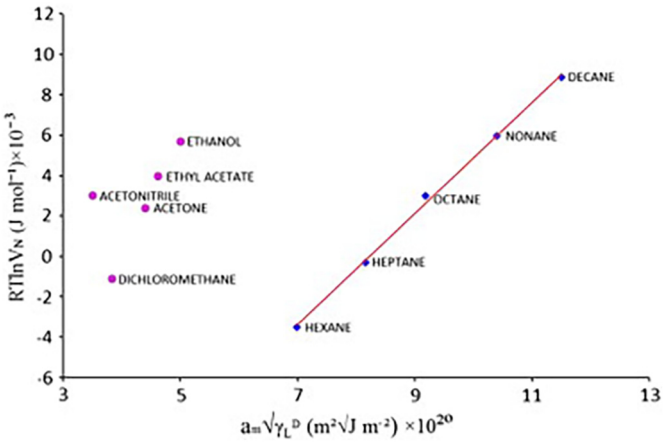

Fig. 7. $RT(\ln(V_n))$ against the carbon number of the alkanes used Dorris-Gray method; the dispersive free energy is determined from the slope. Retrieved from [110].

Regarding the analysis technique itself, the sample of choice is packed into a column, after which a series of alkanes with known dispersive and polar components are injected. The retention volume V_n for each of the alkanes is determined, and $RTln(V_n)$ is plotted against the carbon number of the alkanes. This leads to a linear graph, as illustrated in Fig. 7 for quarts [110]. The dispersive component of the surface free energy can be determined from the slope of the produced graph:

$$\gamma_s^D = \frac{slope^2}{4N^2(a_{CH2})^2\gamma_{CH2}} \quad (20)$$

The polar component of the surface free energy can be determined, for example by the polarisation method [114]. First the specific free energy of adsorption of the different probe molecules (i.e. ΔG^{SP}) is determined from the retention volumes of the polar probe molecules on the sample, from which the molar deformation polarisation P_D follows:

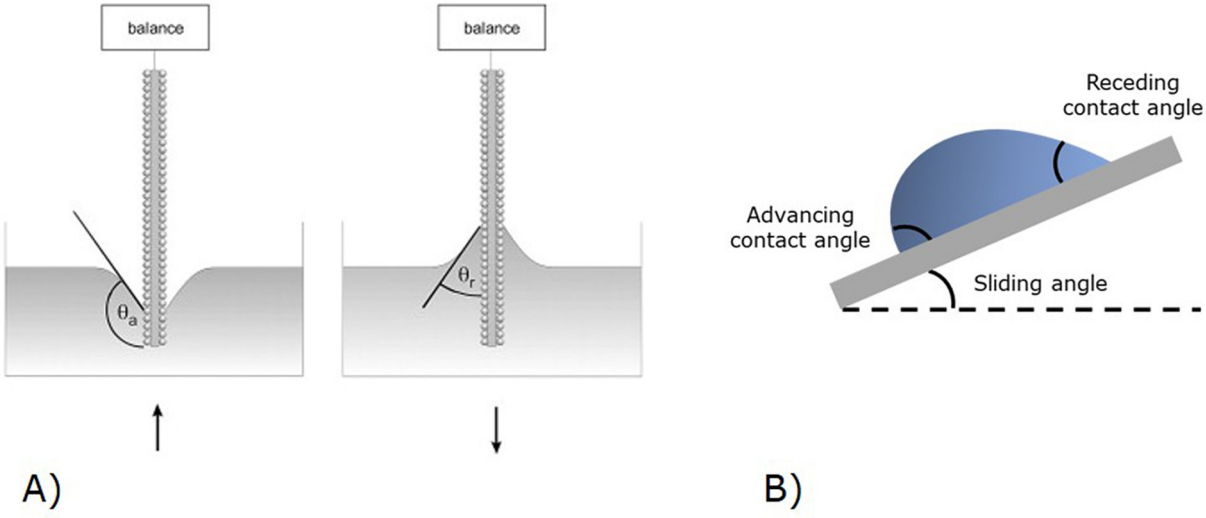

Fig. 6. A schematic illustration of A) the Wilhelmy technique where a plate is covered by particles. During immersion the advancing contact angle is measured, and during withdrawal the receding contact angle. Retrieved from [13] B) the tilting plate technique where a sessile drop is placed on a plate with fixed particles. The drop forms two angles when the plate is tilted, i.e. the advancing contact angle at the lower side of the drop, and the receding contact angle at the upper side of the drop.

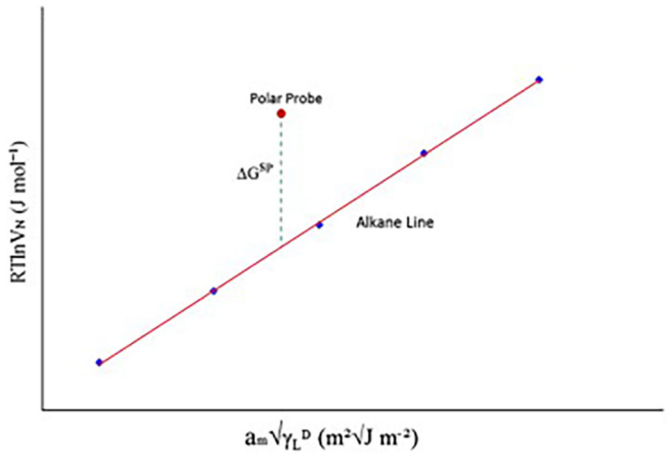

Fig. 8. Schematic representation of $RTln(V_n)$ against the molar deformation polarisation of the probe molecules. The retention volumes of the polar probe molecules are located above the alkane like, from which the total free energy of the compound using the vertical distance between the alkane line and the polar probe. Retrieved from [110].

$$P_D = \frac{M_w^*(r^2-1)}{D^*(r^2+2)} \tag{21}$$

where, M_w is the molecular mass of the probe, r is the refractive index of the probe, and D is the probe liquid density.

Also the $RTln(Vn)$ against PD plot should produce a linear relationship, where the points of the polar probes are located above the alkane line (Fig. 8). The vertical distance between the alkane line, and the polar probe gives the total free energy of the sample of choice. The polar contribution of the surface free energy can then be calculated using Eq. (2).

5.2. Aggregate strength – Static light scattering

Recently, we have developed a method to quantify the bond energy of nanoparticle aggregates [55]. Dispersions containing aggregates of chitin nanocrystals were subjected to ultrasound treatment, from which the energy input was determined calorimetrically, and static light scattering was used to describe the total scattering behaviour of the particles. When plotted against the applied energy input (Fig. 9), Eq. (20) was fitted through the static light scattering data points, from which $E_{aggregate}$ could be calculated. In principle, every mechanical force can be used as long as the nanoparticle aggregates are broken up, and the applied energy input can be quantified.

5.3. Region of the interphase – atomic force microscopy

To date, atomic force microscopy (AFM) is the only device which is able to visualize the interphase, and also quantify its local mechanical properties (e.g. Young's moduli). For nanocomposites commonly either the peak force tapping mode (PF-TM) or intermodulation mode (ImAFM) is used, and will therefore be the focus of this section. It is good to mention that predictive models revolve around the interfacial region.

5.3.1. Peak force tapping mode (PF-TM)

Tapping mode is a commonly applied technique for high-resolution imaging of nanocomposites. To derive more quantitative data about the material itself, the peak force tapping mode (PF-TM) can be used at which the probe tip oscillates at the frequency of the cantilever. The peak force (i.e. the maximum applied force) is precisely controlled and used as a feedback system, and a force separation curve of each tap (i.e. each pixel) is recorded, which gives information about the

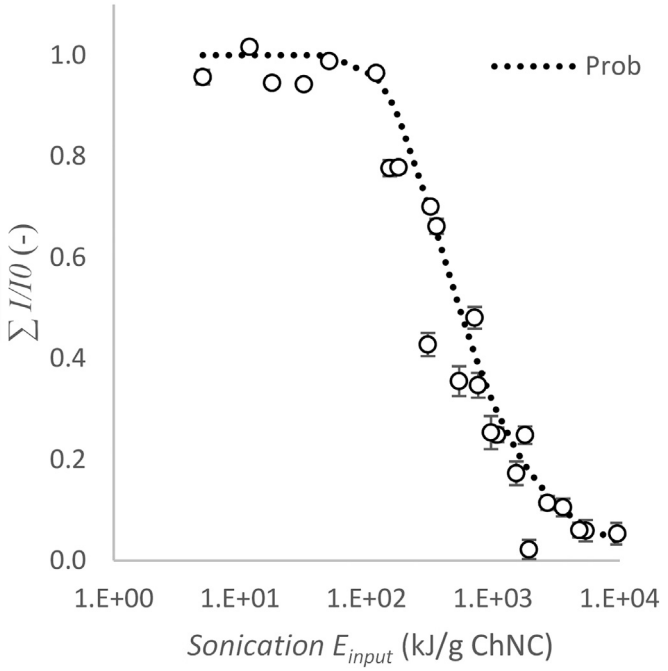

Fig. 9. Normalized total intensity as function of ultra sound energy (E_{input}) in kJ / g ChNC determined via small angle light scattering. Modified from [55].

material properties including deformation, adhesion, modulus, and dissipation. As the height and force curves are derived simultaneously, it enables the creation of material property maps with the same resolution as the height image. Force distance curves need to be cautiously analysed, as they might be distorted by improper spring constant or uncertain shape of the probe. This can be circumvented by using a probe with a known shape and automatic parameter calibration [115].

Fig. 10 gives a schematic representation of the force separation curve obtained during PF-AFM measurements [116]. To translate the force separation curve into different material properties, the Derjaguin-Muller-Toropov model can be fitted through the initial section of the

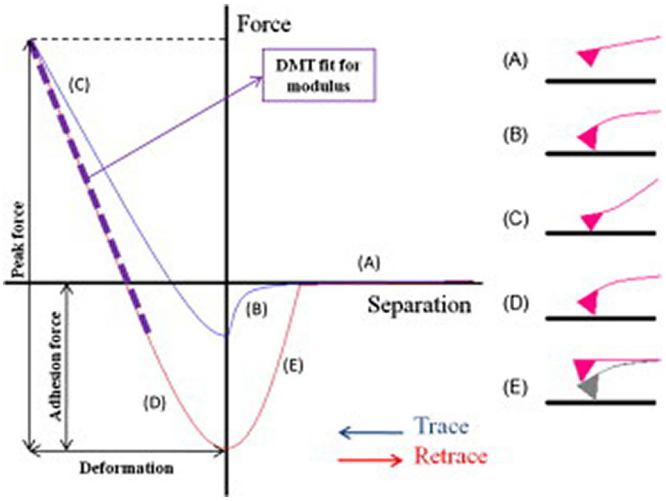

Fig. 10. Schematic representation of the force separation curve obtained in AFM peak force tapping mode. A) the AFM tip approaches the sample and there is no to little force on the tip B) The tip starts to touch the surface as a consequence of attractive tip-surface forces C) A maximum deformation because of maximum tip-surface interactions D) The tip-surface interactions start to become weaker and the tip comes of the surface E) The AFM tip returns to its original position. Retrieved from [69].

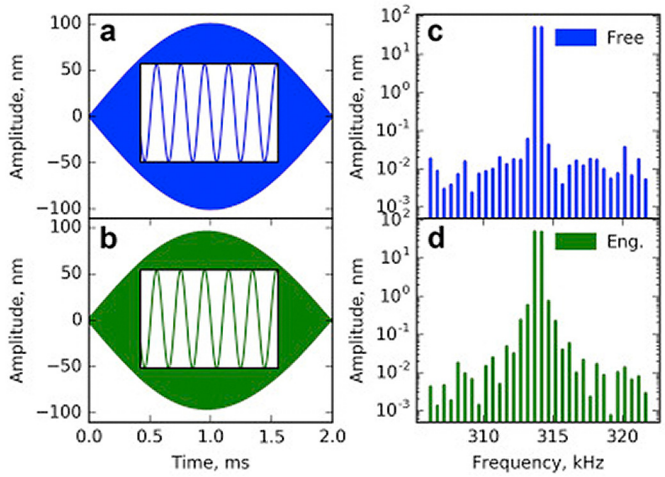

Fig. 11. Schematic overview of free oscillation (upper) and engaged oscillation (bottom) recorded in time (a, b) and frequency domain (c, d). Part a and b show the amplitude of the individual oscillations. Retrieved from [121].

retrace curve [117]. Although other models exist (e.g. Johnson-Kendall-Roberts model [118]), the Derjaguin-Muller-Topopov model is very suitable for nanocomposites because the deformation of the sample is often lower than the tip radius, and adhesion forces are taken into account (in contrast to the Hertz model):

$$F = \frac{4}{3} E^* \sqrt{Rd^3} + F_{adhesion} \tag{22}$$

where F is the force on the tip, R is tip radius, d is the deformation, $F_{adhesion}$ is the force of adhesion between the tip and the sample, and E^* is the reduced elastic modulus. When the Poisson ratio of the sample (v_s) and the tip (v_{tip}) are known, the elastic modulus of the sample can be calculated, assuming that the tip has an infinite elastic modulus (E_{tip}) [119]:

$$E^* = \left(\frac{1-v_s^2}{E_s} + \frac{1-v_{tip}^2}{E_{tip}} \right)^{-1} \tag{23}$$

5.3.2. Inter modulation AFM (ImAFM)

AFM techniques have been extended using multiple frequencies instead of one to excite the probe, i.e. intermodulation AFM (ImAFM) [120].

During the measurement, the cantilever is excited with two frequencies close to the resonance of the cantilever. At the start of the measurement, there are no tip-sample interactions and a free oscillation spectrum is recorded (Fig. 11A and C). When the tip approaches the sample the cantilever is perturbed by a non-linear tip-surface interaction (Fig. 11B and D). Consequently, the two frequencies intermodulate (basically they mix), forming a new frequency near the cantilever resonance, i.e. intermodulation products (IMP), which are recorded. These IMPs contain additional information about the tip-surface interactions, which cannot be acquired by peak force AFM; for instance, the viscous behaviour of the material derived from the energy dissipated from the tip-sample [87]. However, the analysis is less straight forward as for other AFM techniques, and more simulation work on the tip-surface interactions is required to translate these values to e.g. local Youngs moduli [121].

6. Summary and outlook

Addition of nanoparticles to a polymer matrix hold the promise to obtain advanced products with greatly improved properties. In reality, this goal is not often achieved. We find that the options that are explored do not really follow the theoretical frameworks that are available, but are rather trial and error in nature. Nanocomposite design would greatly be helped by a description of the theories that are available and how the essential parameters can be measured, and that is what the current review tries to achieve.

We provide thermodynamic and kinetic approaches to improve nanoparticle dispersion. Next to that, we discussed how nanoparticle – polymer interactions on an atomic scale affect the material properties on a nano, micro, and bulk scale. Furthermore, we identified three parameters which are often overlooked when designing nanocomposites, i.e. the polar and dispersive component of the surface energy of the nanoparticle and polymer, the cohesive bond energy of nanoparticle aggregates, and the quantification of the interphase region once added to the matrix. We finished with a section on how to quantify the latter designing parameters.

Considering these fundamental parameters is one step toward a better understanding of why some nanoparticle – polymer combinations are more successful than others. Most theoretical frameworks correctly describe tendencies of certain effects (e.g. nanoparticle aggregation), but better insight in the actual time frames in which these take place are crucial. As pointed out, thermodynamic and kinetic effects dominate at very different time scales, and depending on their relative importance this will lead to very different materials. To be able to differential between relative importance, we feel that computer simulations could play a very instrumental role, on the condition that the actual values that are used are established correctly by applying the methods that we presented earlier. Our conclusion would be that there is still a world to gain when practical and simulation tools are used symbiotically, and we believe that this will facilitate the design of the advanced materials our society is in dire need of.

Declaration of Competing Interest

The authors declare that they have no known competing financial interests or personal relationships that could have appeared to influence the work reported in this paper.

Acknowledgements

This research was carried out under project number A17020 in the framework of the Research program of the Materials innovation institute (M2i) (www.m2i.nl) supported by the Dutch government.

Appendix A. Supplementary data

Supplementary data to this article can be found online at https://doi.org/10.1016/j.cis.2021.102419.

References

[1] Ma P, Siddiqui NA, Marom G, Kim J. Composites : part a dispersion and functionalization of carbon nanotubes for polymer-based nanocomposites : a review. Compos Part A. 2010;41:1345–67. https://doi.org/10.1016/j.compositesa.2010.07.003.
[2] Zhong BLW. Review on polymer / graphite nanoplatelet nanocomposites; 2011; 5595–614. https://doi.org/10.1007/s10853-011-5572-y.
[3] Oksman K, Aitomäki Y, Mathew AP, Siqueira G, Zhou Q, Butylina S, et al. Review of the recent developments in cellulose nanocomposite processing. Compos Part A Appl Sci Manuf. 2016;83:2–18. https://doi.org/10.1016/j.compositesa.2015.10.041.
[4] Müller K, Bugnicourt E, Latorre M, Jorda M, Echegoyen Sanz Y, Lagaron J, et al. Review on the processing and properties of polymer nanocomposites and nanocoatings and their applications in the packaging. Automot Solar Energy Fields Nanomater. 2017;7:74. https://doi.org/10.3390/nano7040074.

[5] Vasile C. Polymeric nanocomposites and nanocoatings for food packaging : a review; 2018. https://doi.org/10.3390/ma11101834.
[6] Attaran SA, Hassan A, Wahit MU. Materials for food packaging applications based on bio-based polymer nanocomposites : A review; 2017. https://doi.org/10.1177/0892705715588801.
[7] Youssef AM, Youssef AM. Polymer nanocomposites as a new trend for packaging applications polymer nanocomposites as a new trend for packaging applications, 2559; 2013. https://doi.org/10.1080/03602559.2012.762673.
[8] Râpă M, Miteluț AC, Tănase EE, Grosu E, Popescu P, Popa ME, et al. Influence of chitosan on mechanical, thermal, barrier and antimicrobial properties of PLA-biocomposites for food packaging. Compos Part B Eng. 2016;102:112–21. https://doi.org/10.1016/j.compositesb.2016.07.016.
[9] Salaberria AM, Diaz RH, Labidi J, Fernandes SCM. Role of chitin nanocrystals and nanofibers on physical, mechanical and functional properties in thermoplastic starch films. Food Hydrocoll. 2015;46:93–102. https://doi.org/10.1016/j.foodhyd.2014.12.016.
[10] Sahraee S, Milani JM, Ghanbarzadeh B, Hamishehkar H. Physicochemical and antifungal properties of bio-nanocomposite film based on gelatin-chitin nanoparticles. Int J Biol Macromol. 2017;97:373–81. https://doi.org/10.1016/j.ijbiomac.2016.12.066.
[11] Salaberria AM, Diaz RH, Andrés MA, Fernandes SCM, Labidi J. The antifungal activity of functionalized chitin nanocrystals in poly (Lactid acid) films. Materials (Basel). 2017;10:1–16. https://doi.org/10.3390/ma10050546.
[12] Ngo DH, Kim SK. Antioxidant effects of chitin, chitosan, and their derivatives. 1st ed. , 73 Elsevier Inc; 2014. https://doi.org/10.1016/B978-0-12-800268-1.00002-0.
[13] Stöckelhuber KW, Das A, Jurk R, Heinrich G. Contribution of physico-chemical properties of interfaces on dispersibility, adhesion and flocculation of filler particles in rubber. Polymer (Guildf). 2010;51:1954–63. https://doi.org/10.1016/j.polymer.2010.03.013.
[14] Tang Q, Wang F, Guo H, Yang Y, Du Y, Liang J, et al. Effect of coupling agent on surface free energy of organic modified attapulgite (OAT) powders and tensile strength of OAT/ethylene-propylene-diene monomer rubber nanocomposites. Powder Technol. 2015;270:92–7. https://doi.org/10.1016/j.powtec.2014.09.005.
[15] Natarajan B, Li Y, Deng H, Brinson LC, Schadler LS. Effect of interfacial energetics on dispersion and glass transition temperature in polymer nanocomposites. Macromolecules. 2013;46:2833–41. https://doi.org/10.1021/ma302281b.
[16] Khoshkava V, Kamal MR. Effect of surface energy on dispersion and mechanical properties of polymer/nanocrystalline cellulose nanocomposites. Biomacromolecules. 2013;14:3155–63. https://doi.org/10.1021/bm400784j.
[17] Starr FW, Douglas JF, Glotzer SC. Origin of particle clustering in a simulated polymer nanocomposite and its impact on rheology. J Chem Phys. 2003;119:1777–88. https://doi.org/10.1063/1.1580099.
[18] Zhang L, Dong H, Li M, Wang L, Liu Y, Wang L, et al. Fabrication of polylactic acid-modified carbon black composites into improvement of levelness and mechanical properties of spun-dyeing polylactic acid composites membrane. ACS Sustain Chem Eng. 2019;7:688–96. https://doi.org/10.1021/acssuschemeng.8b04264.
[19] Castellano M, Conzatti L, Turturro A, Costa G, Busca G. Influence of the silane modifiers on the surface thermodynamic characteristics and dispersion of the silica into elastomer compounds. J Phys Chem B. 2007;111:4495–502. https://doi.org/10.1021/jp0702144.
[20] Gan L, Liao J, Lin N, Hu C, Wang H, Huang J. Focus on gradientwise control of the surface acetylation of cellulose nanocrystals to optimize mechanical reinforcement for hydrophobic polyester-based nanocomposites. ACS Omega. 2017;2:4725–36. https://doi.org/10.1021/acsomega.7b00532.
[21] Bee SL, Abdullah MAA, Bee ST, Sin LT, Rahmat AR. Polymer nanocomposites based on silylated-montmorillonite: a review. Prog Polym Sci. 2018;85:57–82. https://doi.org/10.1016/j.progpolymsci.2018.07.003.
[22] Karnati SR, Agbo P, Zhang L. Applications of silica nanoparticles in glass/carbon fiber-reinforced epoxy nanocomposite. Compos Commun. 2020;17:32–41. https://doi.org/10.1016/j.coco.2019.11.003.
[23] Xu GR, Wang JN, Li CJ. Strategies for improving the performance of the polyamide thin film composite (PA-TFC) reverse osmosis (RO) membranes: surface modifications and nanoparticles incorporations. Desalination. 2013;328:83–100. https://doi.org/10.1016/j.desal.2013.08.022.
[24] Saravanan N, Rajasekar R, Mahalakshmi S, Sathishkumar TP, Sasikumar K, Sahoo S. Graphene and modified graphene-based polymer nanocomposites - a review. J Reinf Plast Compos. 2014;33:1158–70. https://doi.org/10.1177/0731684414524847.
[25] Liu J, Gao Y, Cao D, Zhang L, Guo Z. Nanoparticle dispersion and aggregation in polymer nanocomposites: insights from molecular dynamics simulation. Langmuir. 2011;27:7926–33. https://doi.org/10.1021/la201073m.
[26] Ray SS, Okamoto M. Polymer / layered silicate nanocomposites : a review from preparation to processing, 28; 2003; 1539–641. https://doi.org/10.1016/j.progpolymsci.2003.08.002.
[27] Ray SS. Springer series in materials science volume 278, Processing of nanocomposites; 2018.
[28] Koval AA, Shevchenko VG, Shchegolikhin AN, Nedorezova PM, Klyamkina AN, Aladyshev AM. Effect of carbon nanotube functionalization on the structural and mechanical properties of polypropylene / MWCNT composites; 2008; 7536–42. https://doi.org/10.1021/ma801599q.
[29] Velasco-santos C, Martı AL, Fisher FT, Ruoff R, Castan VM. Improvement of thermal and mechanical properties of carbon nanotube composites through chemical functionalization; 2003; 4470–5. https://doi.org/10.1021/cm034243c.
[30] Buffa F, Abraham GA, Grady BP, Resasco D. Effect of nanotube functionalization on the properties of single-walled carbon nanotube / polyurethane composites; 2007; 490–501. https://doi.org/10.1002/polb.
[31] Cantor KM, Watts P. Plastics processing. Elsevier. 2011. https://doi.org/10.1016/B978-1-4377-3514-7.10012-1.
[32] Rishi K, Narayanan V, Beaucage G, McGlasson A, Kuppa V, Ilavsky J, et al. A thermal model to describe kinetic dispersion in rubber nanocomposites: the effect of mixing time on dispersion. Polymer (Guildf). 2019;175:272–82. https://doi.org/10.1016/j.polymer.2019.03.044.
[33] Móczó J, Pukánszky B. Polymer micro and nanocomposites: structure, interactions, properties. J Ind Eng Chem. 2008;14:535–63. https://doi.org/10.1016/j.jiec.2008.06.011.
[34] Gaspar H, Teixeira P, Santos R, Fernandes L, Hilliou L, Weir MP, et al. A journey along the extruder with polystyrene:C60Nanocomposites: convergence of feeding formulations into a similar nanomorphology. Macromolecules. 2017;50:3301–12. https://doi.org/10.1021/acs.macromol.6b02283.
[35] Khoshkava V, Kamal MR. Effect of drying conditions on cellulose nanocrystal (CNC) agglomerate porosity and dispersibility in polymer nanocomposites. Powder Technol. 2014;261:288–98. https://doi.org/10.1016/j.powtec.2014.04.016.
[36] Abdallah W, Kamal MR. Influence of process variables on physical characteristics of spray freeze dried cellulose nanocrystals. Cellulose. 2018;25:5711–30. https://doi.org/10.1007/s10570-018-1975-0.
[37] Beuguel Q, Tavares JR, Carreau PJ, Heuzey MC. Ultrasonication of spray- and freeze-dried cellulose nanocrystals in water. J Colloid Interface Sci. 2018;516:23–33. https://doi.org/10.1016/j.jcis.2018.01.035.
[38] Abdallah W, Tan V, Kamal MR. The effect of spray-freeze drying of montmorillonite on the morphology, dispersion, and crystallization in polypropylene nanocomposites. Polym Eng Sci. 2020;60:168–79. https://doi.org/10.1002/pen.25270.
[39] Owens DK, De Nemours EIP, Film S. Estimation of 1969, 13; 1969; 1741–7.
[40] Good RJ, Girifalco LA. A theory for estimation of surface and interfacial energies. III. Estimation of surface energies of solids from contact angle data. J Phys Chem. 1960;64:561–5. https://doi.org/10.1021/j100834a012.
[41] Cheung O, Zhang P, Frykstrand S, Zheng H, Yang T, Sommariva M, et al. Nanostructure and pore size control of template-free synthesised mesoporous magnesium carbonate. RSC Adv. 2016;6:74241–9. https://doi.org/10.1039/c6ra14171d.
[42] Shavit A, Riggleman RA. The dynamics of unentangled polymers during capillary rise infiltration into a nanoparticle packing. Soft Matter. 2015;11:8285–95. https://doi.org/10.1039/c5sm01866h.
[43] Supple S, Quirke N. Rapid imbibition of fluids in carbon nanotubes, 90; 2003; 1–4. https://doi.org/10.1103/PhysRevLett.90.214501.
[44] Yao Y, Butt HJ, Floudas G, Zhou J, Doi M. Theory on capillary filling of polymer melts in nanopores. Macromol Rapid Commun. 2018;39:1–5. https://doi.org/10.1002/marc.201800087.
[45] Dimitrov DI, Milchev A, Binder K. Capillary rise in nanopores: molecular dynamics evidence for the Lucas-Washburn equation n.d,1; 2007; 17–20.
[46] Hu G, Cao B. Flows of polymer melts through nanopores: experiments and modelling. J Therm Sci Technol. 2013;8:363–9. https://doi.org/10.1299/jtst.8.363.
[47] Xiao F, Xu H, Li XY, Wang D. Modeling particle-size distribution dynamics in a shear-induced breakage process with an improved breakage kernel: importance of the internal bonds. Colloids Surf A Physicochem Eng Asp. 2015;468:87–94. https://doi.org/10.1016/j.colsurfa.2014.11.060.
[48] Odriozola G, Schmitt A, Moncho-Jordá A, Callejas-Fernández J, Martínez-García R, Leone R, et al. Constant bond breakup probability model for reversible aggregation processes. Phys Rev E. 2002;65:1–8. https://doi.org/10.1103/PhysRevE.65.031405.
[49] Duan B, Chang C, Ding B, Cai J, Xu M, Feng S, et al. High strength films with gas-barrier fabricated from chitin solution dissolved at low temperature. J Mater Chem A. 2013;1:1867–74. https://doi.org/10.1039/c2ta00068g.
[50] Calderón BA, McCaughey MS, Thompson CW, Barinelli VL, Sobkowicz MJ. Evaluating the influence of specific mechanical energy on biopolymer blends prepared via high-speed reactive extrusion. ACS Appl Polym Mater. 2019;1:1410–9. https://doi.org/10.1021/acsapm.9b00177.
[51] Domenech T, Peuvrel-Disdier E, Vergnes B. The importance of specific mechanical energy during twin screw extrusion of organoclay based polypropylene nanocomposites. Compos Sci Technol. 2013;75:7–14. https://doi.org/10.1016/j.compscitech.2012.11.016.
[52] Hassinger I, Li X, Zhao H, Xu H, Huang Y, Prasad A, et al. Toward the development of a quantitative tool for predicting dispersion of nanocomposites under non-equilibrium processing conditions. J Mater Sci. 2016;51:4238–49. https://doi.org/10.1007/s10853-015-9698-1.
[53] Mack C, Sathyanarayana S, Weiss P, Mikonsaari I, Hübner C, Henning F, et al. Twin-screw extrusion of multi walled carbon nanotubes reinforced polycarbonate composites: investigation of electrical and mechanical properties. IOP Conf Ser Mater Sci Eng. 2012;40. https://doi.org/10.1088/1757-899X/40/1/012020.
[54] Villmow T, Kretzschmar B, Pötschke P. Influence of screw configuration, residence time, and specific mechanical energy in twin-screw extrusion of polycaprolactone/multi-walled carbon nanotube composites. Compos Sci Technol. 2010;70:2045–55. https://doi.org/10.1016/j.compscitech.2010.07.021.
[55] Colijn I, Fokkink R, Schroen K. Quantification of energy input required for chitin nanocrystal aggregate size reduction through ultrasound 2020. Manuscript submitted for publication; 2021.
[56] Diemer J, Chilles C, Colbert J, Miri T, Ingram A, David P, et al. Flow visualisation in co-rotating twin screw extruders: positron emission particle tracking and numerical particle trajectories. Int Polym Process. 2011;26:540–50. https://doi.org/10.3139/217.2475.
[57] Wagner JR, Mount EM, Giles HF. Plastic behavior in the extruder. Extrusion. 2014:47–70. https://doi.org/10.1016/b978-1-4377-3481-2.00004-1.
[58] Xu HN, Tang YY, Ouyang XK. Shear-induced breakup of cellulose nanocrystal aggregates. Langmuir. 2017;33:235–42. https://doi.org/10.1021/acs.langmuir.6b03807.

[59] Vilaverde C, Santos RM, Paiva MC, Covas JA. Dispersion and re-agglomeration of graphite nanoplates in polypropylene melts under controlled flow conditions. Compos Part A Appl Sci Manuf. 2015;78:143–51. https://doi.org/10.1016/j.compositesa.2015.08.010.
[60] Wang T, Keddie JL. Design and fabrication of colloidal polymer nanocomposites. Adv Colloid Interface Sci. 2009;147–148:319–32. https://doi.org/10.1016/j.cis.2008.06.002.
[61] Lee G. Physical chemistry of foods. vol. 57New York: Marcel Dekker inc.; 2004. https://doi.org/10.1016/j.ejpb.2003.10.013.
[62] Shen XJ, Yang S, Shen JX, Ma JL, Wu YQ, Zeng XL, et al. Improved mechanical and antibacterial properties of silver-graphene oxide hybrid/polylactid acid composites by in-situ polymerization. Ind Crop Prod. 2019;130:571–9. https://doi.org/10.1016/j.indcrop.2019.01.018.
[63] Luong ND, Hippi U, Korhonen JT, Soininen AJ, Ruokolainen J, Johansson LS, et al. Enhanced mechanical and electrical properties of polyimide film by graphene sheets via in situ polymerization. Polymer (Guildf). 2011;52:5237–42. https://doi.org/10.1016/j.polymer.2011.09.033.
[64] Qin Y, Zhang S, Yu J, Yang J, Xiong L, Sun Q. Effects of chitin nano-whiskers on the antibacterial and physicochemical properties of maize starch films. Carbohydr Polym. 2016;147:372–8. https://doi.org/10.1016/j.carbpol.2016.03.095.
[65] Nunes RCR, Fonseca JLC, Pereira MR. Polymer-filler interactions and mechanical properties of a polyurethane elastomer. Polym Test. 2000;19:93–103. https://doi.org/10.1016/S0142-9418(98)00075-0.
[66] Nunes RCR, Pereira RA, Fonseca JLC, Pereira MR. X-ray studies on compositions of polyurethane and silica. Polym Test. 2001;20:707–12. https://doi.org/10.1016/S0142-9418(01)00007-1.
[67] Singh RP, Aggarwal P. Effect of nanosilica on the properties of cement mortar. Cem Int. 2015;13:65–70.
[68] Bistričić L, Baranović G, Leskovac M, Bajsić EG. Hydrogen bonding and mechanical properties of thin films of polyether-based polyurethane-silica nanocomposites. Eur Polym J. 2010;46:1975–87. https://doi.org/10.1016/j.eurpolymj.2010.08.001.
[69] Pakzad A, Simonsen J, Yassar RS. Gradient of nanomechanical properties in the interphase of cellulose nanocrystal composites. Compos Sci Technol. 2012;72:314–9. https://doi.org/10.1016/j.compscitech.2011.11.020.
[70] Wong M, Paramsothy M, Xu XJ, Ren Y, Li S, Liao K. Physical interactions at carbon nanotube-polymer interface, 44; 2003; 7757–64. https://doi.org/10.1016/j.polymer.2003.10.011.
[71] Tan H, Jiang LY, Huang Y, Liu B, Hwang KC. The effect of van der Waals-based interface cohesive law on carbon nanotube-reinforced composite materials. Compos Sci Technol. 2007;67:2941–6. https://doi.org/10.1016/j.compscitech.2007.05.016.
[72] Li C, Chou T. SCIENCE AND Multiscale modeling of compressive behavior of carbon nanotube / polymer composites, 66; 2006; 2409–14. https://doi.org/10.1016/j.compscitech.2006.01.013.
[73] Panhuis M, Maiti A, Dalton AB, Van Den Noort A, Coleman JN, McCarthy B, et al. Selective interaction in a polymer-single-wall carbon nanotube composite. J Phys Chem B. 2003;107:478–82. https://doi.org/10.1021/jp026470s.
[74] Rahmat M. Carbon nanotube – polymer interaction in 2011; 2011.
[75] Gou J, Liang Z, Zhang C, Wang B. Computational analysis of effect of single-walled carbon nanotube rope on molecular interaction and load transfer of nanocomposites. Compos Part B Eng. 2005;36:524–33. https://doi.org/10.1016/j.compositesb.2005.02.004.
[76] Odent J, Raquez JM, Dubois P, Giannelis EP. Ultra-stretchable ionic nanocomposites: from dynamic bonding to multi-responsive behavior. J Mater Chem A. 2017;5:13357–63. https://doi.org/10.1039/c7ta04101b.
[77] Karatrantos A, Koutsawa Y, Dubois P, Clarke N, Kröger M. Miscibility and nanoparticle diffusion in ionic nanocomposites n.d ; 2018; 1–16. https://doi.org/10.3390/polym10091010.
[78] van Zanten JH, Wallace WE, Wu W. Favorable substrate interactions. Phys Rev E. 1996;53:2053–6.
[79] Fryer DS, Peters RD, Kim EJ, Tomaszewski JE, De Pablo JJ, Nealey PF, et al. Dependence of the glass transition temperature of polymer films on interfacial energy and thickness. Macromolecules. 2001;34:5627–34. https://doi.org/10.1021/ma001932q.
[80] Desai T, Keblinski P, Kumar SK. Molecular dynamics simulations of polymer transport in nanocomposites. J Chem Phys. 2005;122. https://doi.org/10.1063/1.1874852.
[81] Long D, Lequeux F. Heterogeneous dynamics at the glass transition in van der Waals liquids, in the bulk and in thin films. Eur Phys J E. 2001;4:371–87. https://doi.org/10.1007/s101890170120.
[82] Liu H, Brinson LC. Reinforcing efficiency of nanoparticles: a simple comparison for polymer nanocomposites. Compos Sci Technol. 2008;68:1502–12. https://doi.org/10.1016/j.compscitech.2007.10.033.
[83] Phys JC, Starr FW, Emamy H, Betancourt BAP, Vargas-lara F, Douglas JF. The interfacial zone in thin polymer films and around nanoparticles in polymer nanocomposites The interfacial zone in thin polymer films and around nanoparticles in polymer nanocomposites, 124705; 2019. https://doi.org/10.1063/1.5119269.
[84] Houssat M, Lahoud Dignat N, Cambronne JP, Diaham S. AFM measurements of polyimide/silicon nitride nanocomposite interphase. IEEE Trans Nanotechnol. 2018;17:1146–50. https://doi.org/10.1109/TNANO.2018.2867159.
[85] Huang H. Electrochemical application and AFM characterization of nanocomposites: focus on interphase properties; 2017.
[86] Voyiatzis E, Rahimi M, Müller-Plathe F, Böhm MC. How thick is the polymer interphase in nanocomposites? Probing it by local stress anisotropy and gas solubility. Macromolecules. 2014;47:7878–89. https://doi.org/10.1021/ma500556q.
[87] Khorasani MGZ, Silbernagl D, Platz D, Sturm H. Insights into nano-scale physical and mechanical properties of epoxy/boehmite nanocomposite using different AFM modes. Polymers (Basel). 2019;11. https://doi.org/10.3390/polym11020235.
[88] McArthur SL. Thin films of vanadium oxide grown on vanadium metal. Surf Interface Anal. 2006;38:1380–5. https://doi.org/10.1002/sia.
[89] Zhang M, Askar S, Torkelson JM, Brinson LC. Stiffness gradients in glassy polymer model Nanocomposites: comparisons of quantitative characterization by fluorescence spectroscopy and atomic force microscopy. Macromolecules. 2017;50:5447–58. https://doi.org/10.1021/acs.macromol.7b00917.
[90] Scaffaro R, Botta L, Lopresti F, Maio A, Sutera F. Polysaccharide nanocrystals as fillers for PLA based nanocomposites. Cellulose. 2017;24:447–78. https://doi.org/10.1007/s10570-016-1143-3.
[91] John Lewis T. Nano-composite dielectrics: the dielectric nature of the nano-particle environment. IEEJ Trans Fundam Mater. 2006;126:1020–30. https://doi.org/10.1541/ieejfms.126.1020.
[92] Tanaka T. Interpretation of several key phenomena peculiar to nano dielectrics in terms of a multi-core model. Annu. rep. - conf. electr. insul. dielectr. phenomena. CEIDP; 2006; 298–301. https://doi.org/10.1109/CEIDP.2006.311928.
[93] Amraei J, Jam JE, Arab B, Firouz-Abadi RD. Modeling the interphase region in carbon nanotube- reinforced polymer nanocomposites; 2019. https://doi.org/10.1002/pc.24950.
[94] Maghsoudlou MA, Barbaz Isfahani R, Saber-Samandari S, Sadighi M. Effect of interphase, curvature and agglomeration of SWCNTs on mechanical properties of polymer-based nanocomposites: experimental and numerical investigations. Compos Part B Eng. 2019;175:107119. https://doi.org/10.1016/j.compositesb.2019.107119.
[95] Hu H, Onyebueke L, Abatan A. Characterizing and modeling mechanical properties of nanocomposites-review and evaluation. J Miner Mater Charact Eng. 2010;09:275–319. https://doi.org/10.4236/jmmce.2010.94022.
[96] Zare Y. Development of Halpin-Tsai model for polymer nanocomposites assuming interphase properties and nanofiller size. Polym Test. 2016;51:69–73. https://doi.org/10.1016/j.polymertesting.2016.02.010.
[97] Wang Y, Zhang Y, Zhao H, Li X, Huang Y, Schadler LS, et al. Identifying interphase properties in polymer nanocomposites using adaptive optimization. Compos Sci Technol. 2018;162:146–55. https://doi.org/10.1016/j.compscitech.2018.04.017.
[98] Boutaleb S, Zaïri F, Mesbah A, Naït-abdelaziz M, Gloaguen JM, Boukharouba T, et al. International journal of solids and structures micromechanics-based modelling of stiffness and yield stress for silica / polymer nanocomposites. Int J Solids Struct. 2009;46:1716–26. https://doi.org/10.1016/j.ijsolstr.2008.12.011.
[99] Li X, Zhang M, Wang Y, Prasad A, Chen W, Schadler L, et al. Rethinking interphase representations for modeling viscoelastic properties for polymer nanocomposites. Materialia. 2019;6:100277. https://doi.org/10.1016/j.mtla.2019.100277.
[100] Khoshkava V, Ghasemi H, Kamal MR. Thermochimica Acta effect of cellulose nanocrystals (CNC) on isothermal crystallization kinetics of polypropylene. Thermochim Acta. 2015;608:30–9. https://doi.org/10.1016/j.tca.2015.04.007.
[101] Kim SH, Ahn SH, Hirai T. Crystallization kinetics and nucleation activity of silica nanoparticle-filled poly(ethylene 2,6-naphthalate). Polymer (Guildf). 2003;44:5625–34. https://doi.org/10.1016/S0032-3861(03)00623-2.
[102] Yuan Q, Awate S, Misra RDK. Nonisothermal crystallization behavior of polypropylene-clay nanocomposites. Eur Polym J. 2006;42:1994–2003. https://doi.org/10.1016/j.eurpolymj.2006.03.012.
[103] Bhattacharyya AR, Sreekumar TV, Liu T, Kumar S, Ericson LM, Hauge RH, et al. Crystallization and orientation studies in polypropylene/single wall carbon nanotube composite. Polymer (Guildf). 2003;44:2373–7. https://doi.org/10.1016/S0032-3861(03)00073-9.
[104] Pangelinan AB, Mccullough RL, Kelley MJ. Fiber-matrix interactions in thermoplastic composites. J Thermoplast Compos Mater. 1994;7:192–207. https://doi.org/10.1177/089270579400700302.
[105] Zitzenbacher G, Dirnberger H, Längauer M, Holzer C. Calculation of the contact angle of polymer melts on tool surfaces from viscosity parameters. Polymers (Basel). 2017;10. https://doi.org/10.3390/polym10010038.
[106] Kamal MR, Calderon JU, Lennox BR. Surface energy of modified nanoclays and its effect on polymer/clay nanocomposites. J Adhes Sci Technol. 2009;23:663–88. https://doi.org/10.1163/156856108X379164.
[107] Fowkes FM. Donor-acceptor interactions at interfaces. J Adhes Dent. 1972;4:155–9. https://doi.org/10.1080/00218467208072219.
[108] Ã AR. Analysis for determining surface free energy uncertainty by the Owen – Wendt method. Int J Adhes Adhes. 2009;29:451–7. https://doi.org/10.1016/j.ijadhadh.2008.09.008.
[109] Chau TT, Bruckard WJ, Koh PTL, Nguyen AV. A review of factors that affect contact angle and implications for flotation practice. Adv Colloid Interface Sci. 2009;150:106–15. https://doi.org/10.1016/j.cis.2009.07.003.
[110] Mohammadi-Jam S, Waters KE. Inverse gas chromatography applications: a review. Adv Colloid Interface Sci. 2014;212:21–44. https://doi.org/10.1016/j.cis.2014.07.002.
[111] Dorris GM, Gray DG. Adsorption of n-alkanes at zero surface coverage on cellulose paper and wood fibers. J Colloid Interface Sci. 1980;77:353–62. https://doi.org/10.1016/0021-9797(80)90304-5.
[112] Schultz J, Lavielle L, Martin C. Interfacial properties of carbon fibers - epoxy matrix composites, 58; 1988.
[113] Shi B, Wang Y, Jia L. Comparison of Dorris-Gray and Schultz methods for the calculation of surface dispersive free energy by inverse gas chromatography. J Chromatogr A. 2011;1218:860–2. https://doi.org/10.1016/j.chroma.2010.12.050.
[114] Dong S, Brendle M, Donnet. Study of solid surface polarity by inverse gas chromatography at infinite dilution. Chromatographia. 1989;28:469–72.

[115] Xu K, Sun W, Shao Y, Wei F, Zhang X, Wang W, et al. Recent development of PeakForce tapping mode atomic force microscopy and its applications on nanoscience. Nanotechnol Rev. 2018;7:605–21. https://doi.org/10.1515/ntrev-2018-0086.
[116] Pittenger B, Erina NCS. Bruker application note 128: Quantitative mechanical mapping at nanosclae with peak force QNM; 2009.
[117] Derjaguin BV, Muller VM, Toporov YP. Effect of contact deformations on the adhesion of particles. J Colloid Interface Sci. 1975;53:314–26. https://doi.org/10.1016/0021-9797(75)90018-1.
[118] Section SP, Railways B, Centre T, Physics S. Surface energy and the contact of elastic solids, 313; 1971; 301–13.
[119] Smolyakov G, Pruvost S, Cardoso L, Alonso B, Belamie E, Duchet-Rumeau J. AFM PeakForce QNM mode: evidencing nanometre-scale mechanical properties of chitin-silica hybrid nanocomposites. Carbohydr Polym. 2016;151:373–80. https://doi.org/10.1016/j.carbpol.2016.05.042.
[120] Platz D, Thoĺn EA, Pesen D, Haviland DB. Intermodulation atomic force microscopy. Appl Phys Lett. 2008;92. https://doi.org/10.1063/1.2909569.
[121] Huang H, Dobryden I, Thorén PA, Ejenstam L, Pan J, Fielden ML, et al. Local surface mechanical properties of PDMS-silica nanocomposite probed with intermodulation AFM. Compos Sci Technol. 2017;150:111–9. https://doi.org/10.1016/j.compscitech.2017.07.013.